Physical Adsorption and Charge Transfer of Molecular Br_2 on Graphene

Zheyuan Chen,[†,*] Pierre Darancet,[‡] Lei Wang,[§] Andrew C. Crowther,[∥] Yuanda Gao,[§] Cory R. Dean,[§,⊥,#] Takashi Taniguchi,[▽] Kenji Watanabe,[▽] James Hone,[§] Chris A. Marianetti,[‡] and Louis E. Brus[†]

[†]Department of Chemistry, [‡]Department of Applied Physics and Applied Mathematics, [§]Department of Mechanical Engineering, and [⊥]Department of Electrical Engineering, Columbia University, New York, New York 10027, United States, [∥]Department of Chemistry, Barnard College, New York, New York 10025, United States, [#]Department of Physics, The City College of New York, New York, New York 10031, United States, and [▽]Advanced Materials Laboratory, National Institute for Materials Science, 1-1 Namiki, Tsukuba 305-0044, Japan

ABSTRACT We present a detailed study of gaseous Br_2 adsorption and charge transfer on graphene, combining *in situ* Raman spectroscopy and density functional theory (DFT). When graphene is encapsulated by hexagonal boron nitride (h-BN) layers on both sides, in a h-BN/graphene/h-BN sandwich structure, it is protected from doping by strongly oxidizing Br_2. Graphene supported on only one side by h-BN shows strong hole doping by adsorbed Br_2. Using Raman spectroscopy, we determine the graphene charge density as a function of pressure. DFT calculations reveal the variation in charge transfer per adsorbed molecule as a function of coverage. The molecular adsorption isotherm (coverage *versus* pressure) is obtained by combining Raman spectra with DFT calculations. The Fowler–Guggenheim isotherm fits better than the Langmuir isotherm. The fitting yields the adsorption equilibrium constant (~0.31 $Torr^{-1}$) and repulsive lateral interaction (~20 meV) between adsorbed Br_2 molecules. The Br_2 molecule binding energy is ~0.35 eV. We estimate that at monolayer coverage each Br_2 molecule accepts 0.09 e^- from single-layer graphene. If graphene is supported on SiO_2 instead of h-BN, a threshold pressure is observed for diffusion of Br_2 along the (somewhat rough) SiO_2/graphene interface. At high pressure, graphene supported on SiO_2 is doped by adsorbed Br_2 on both sides.

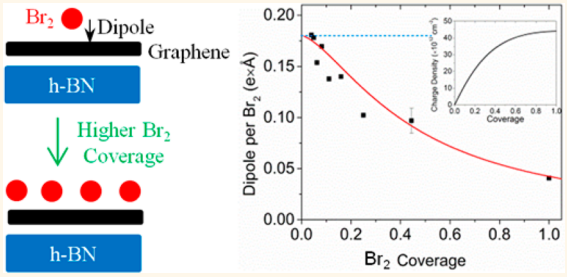

KEYWORDS: graphene · hexagonal boron nitride · bromine · adsorption isotherm · charge transfer · band gap · Raman spectroscopy

Graphene has attracted significant interest as a robust 2-dimensional material of only one-atom thickness and extremely high carrier mobility.[1−4] Hexagonal single-layer graphene (SLG) and bilayer graphene (BLG) are semimetals with zero bandgap. Environmental effects which lower symmetry and/or donate charge can substantially change graphene electronic properties. For example, a perpendicular electric field in BLG breaks inversion symmetry and creates a static potential difference between the two layers.[5,6] This symmetry breaking leads to the formation of tunable band gap whose magnitude depends proportionally on the potential difference between the two SLGs.[5−8] Such potential differences can be created by an electrostatic gate in a field-effect transistor (FET) geometry, or by one-sided molecular adsorption and charge transfer.[9−11] Adsorption can cause substantial charge transfer; for example, the Fermi level of SLG shifts by more than 1 eV due to electron donation from adsorbed potassium monolayers.[12] This shift also creates an optical absorption threshold of more than 2 eV. While adsorption-induced charge transfer can be large, note that incomplete or amorphous adsorbed layers can deteriorate the high mobility of graphene by introducing scattering centers.

A high-level of SLG hole doping is created by electron transfer to adsorbed halogen molecules.[13] Bromine is especially interesting in this regard. The lattice structure of solid molecular Br_2 is commensurate with that of graphene, giving rise to the observed crystalline Br_2 layers that can be intercalated into bulk graphite.[14] This intercalated crystalline layer can act as a modulation doping layer in bulk graphite, leaving intact the high mobility.[15−17] Adlayers created by gaseous Br_2 adsorption also strongly hole dope SLG and BLG. Such adsorption can be either one-sided or two-sided. Generally speaking, a tight seal between hexagonal

* Address correspondence to zc2145@columbia.edu.

Received for review January 13, 2014 and accepted February 14, 2014.

Published online February 14, 2014
10.1021/nn500265f

boron nitride (h-BN) and graphene prevents gas diffusion along their van der Waals interface. Asymmetric doping of BLG on h-BN exposed to high pressure (*ca.* 100 Torr) gaseous Br_2 both dopes the sample and opens a static bandgap, with a distinctive feature in the Raman spectrum —— the splitting of the G peak into two components.[18,19]

In this paper, we try to understand more deeply the fundamental adsorption and charge transfer processes of gaseous Br_2 on SLG as a function of coverage. We use graphene Raman scattering to characterize charge transfer, as the correlation between Raman G peak position and graphene charge density is well documented.[20−23] From the experimental coverage dependence of charge transfer, we derive the molecular adsorption isotherm. We perform a theoretical DFT study of Br_2 adsorption on graphene to model and calibrate how charge transfer per Br_2 molecule varies with coverage. We study both one-sided adsorption on h-BN and two-sided adsorption on SiO_2. To our knowledge, this type of in-depth study of molecular adsorption and charge transfer on graphene has not been previously attempted.

RESULTS AND DISCUSSION

We first studied the adsorption of Br_2 on the h-BN/SLG/h-BN sandwich structure, in which graphene is encapsulated by h-BN on both sides. Encapsulation of graphene inside this sandwich structure preserves the intrinsic properties of graphene from the degradation caused by an oxide substrate and by high temperature processing-induced environmental doping.[24] Here, we report that such encapsulation also prevents the doping of graphene by the strong oxidant Br_2. The exposure of h-BN/SLG/h-BN to ~100 Torr Br_2 gas induces a negligible change (<1 cm^{-1}) in G peak position (see Supporting Information), compared with a large shift (~44 cm^{-1}) for adsorption occurring on SiO_2 supported bare graphene.[13] The negligible change means that the charge density of graphene remains the same after Br_2 exposure in the sandwich structure. Thus, Br_2 does not diffuse into either of the van der Waals interfaces between graphene and H-BN. Br_2 must adsorb to some extent on the outer h-BN surfaces, but there is no evidence of any charge transfer through h-BN.

It is interesting to compare this sandwich structure to the case of three-layer thick graphene. Br_2 at *ca.* 100 Torr diffuses into (*i.e.*, intercalates) one, but not both, interior interface in the three layer graphene structure, in addition to adsorbing onto both outer surfaces.[13] The net result is that all three graphene layers are strongly hole doped by direct contact with Br_2. By comparison, the strongly oxidizing species NO_2 adsorbs onto graphene, but does not intercalate. Three layer graphene exposed to gaseous NO_2 shows strong doping of the two outer layers in direct contact with

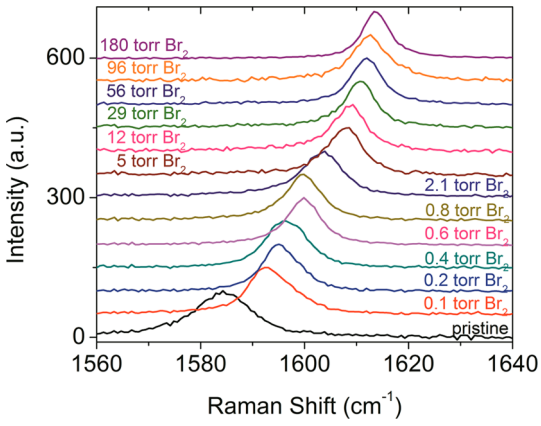

Figure 1. Raman spectra of h-BN supported single-layer graphene exposed to Br_2 of various pressures. The same graphene sample was exposed to the lowest pressure Br_2 (~0.1 Torr) first and higher pressure gradually. The corresponding pressure is indicated in the same color as the spectrum.

adsorbed NO_2, and modest doping of the interior layer not in direct contact.[17] These experiments show the very strongly insulating nature of single h-BN sheets on graphene. H-BN has a 5.97 eV band gap,[25] and the contacting h-BN/graphene flat van der Waals layers conform to each other with similar structure and lattice constant.[26−28] The little interaction between h-BN and Br_2 cannot compensate the intercalation energy of Br_2 into the interface.

We now focus on h-BN supported graphene which has one side exposed for Br_2 adsorption. This is different from SiO_2-supported graphene which adsorbs Br_2 on both sides at high pressure, as described later. We monitored the shift of the graphene Raman G peak as a function of Br_2 pressure. At each Br_2 pressure, the adsorbed phase of Br_2 on graphene surface reaches dynamic equilibrium with the gas phase. As the pressure increases, the adsorbed Br_2 coverage should increase correspondingly. In Figure 1 we observe a monotonic increase in the graphene G peak position with pressure.

To determine the charge density of graphene from the G peak position, we carefully examined several reports of G peak position at known graphene charge density, as controlled by FET back gating or electrolyte top gating.[20−23] Two of them give the same slope (42.9 cm^{-1}/eV) of G peak position *versus* Fermi energy shift.[20,23] We use the Yan *et al.* data which has the correct intercept (1580.5 cm^{-1}) at negligible charge density.[20] In support of the Yan *et al.* calibration, note that in a previous study of reflective optical contrast of graphene doped by NO_2,[17] the use of the Yan *et al.* Raman data gave the Fermi level shift close to the half of the optical absorption threshold, as predicted by theory.

In Figure 2, we plot the hole charge density of graphene as a function of Br_2 pressure, using the Yan *et al.* calibration. There should be two separate

molecular effects in Figure 2. One is the Br_2 coverage as a function of pressure (*i.e.*, the adsorption isotherm), and the other is the charge transfer per adsorbed Br_2 as a function of coverage. We do not have a direct, independent measurement of coverage, which would be difficult to obtain in the presence of a corrosive gas like Br_2 at high pressure. Thus, we have performed a DFT study of Br_2 on graphene, to understand the net charge transfer per molecule as a function of coverage.

We calculate the electronic density and changes in work function of graphene supercells, made of one adsorbed Br_2 at the center of different cells, from 2×2 to 10×10 unit cells in size. Dresselhaus suggested that 1 Br_2 molecule on 2×2 unit cells (C_8Br_2) corresponds to monolayer coverage.[14] Thus, the different sizes of supercells represent different Br_2 coverages, varying from 4% to 100%. In principle, Br_2 might adsorb either perpendicular or parallel to graphene. Previous Br_2/graphene DFT studies with a van der Waals-corrected functional[29] show that in-plane geometries are 60−90 meV more stable than perpendicular geometries. Boltzmann factors at room temperature for the binding energies reported in ref 29 suggest Br_2 lays in the parallel configurations 97% of the time, and that the perpendicular geometries can be neglected. Moreover, the dominant van der Waals contribution to the binding energy of ref 29 (~97% of the binding energy) for the intermediate coverage regime ($C_{24}Br_2$ and $C_{32}Br_2$) suggests that Br_2 geometries will be weakly dependent on the coverage. The five different in-plane geometries of ref 29 are then considered in the following for all coverages. Unless indicated otherwise, the different properties reported in the next are averaged over them. The charge densities are calculated using the work function change on the graphene-side upon adsorption[21] with the GGA-PBE Fermi velocity.

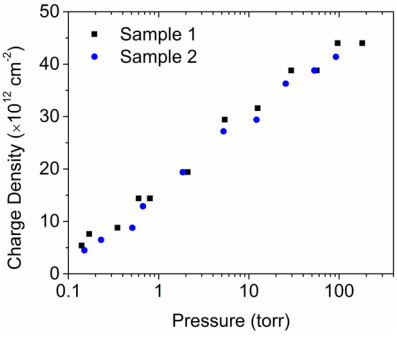

Figure 2. Charge density of graphene on h-BN as a function of Br_2 pressure. The sets of black squares were extracted from G peak positions of Raman spectra shown in Figure 1. A second sample (blue circles) was measured independently. Pressure is in logarithmic scale as the variation is over 3 orders of magnitude.

In Figure 3, we show the computed hole densities along with their corresponding energy shifts in work function, for one of the geometries. The hole density does not increase linearly with coverage, indicating that the charge transfer per molecule decrease s as coverage increases. Comparing with a linear extrapolation of the low-coverage charge transfer, we find that the charge transfer at full coverage is reduced by 70%. This coverage dependence of the charge transfer becomes significant for coverages as low as 11%. The inset shows the change of graphene work function which increases monotonically with the Br_2 coverage and reaches a maximum of ~0.31 eV at monolayer

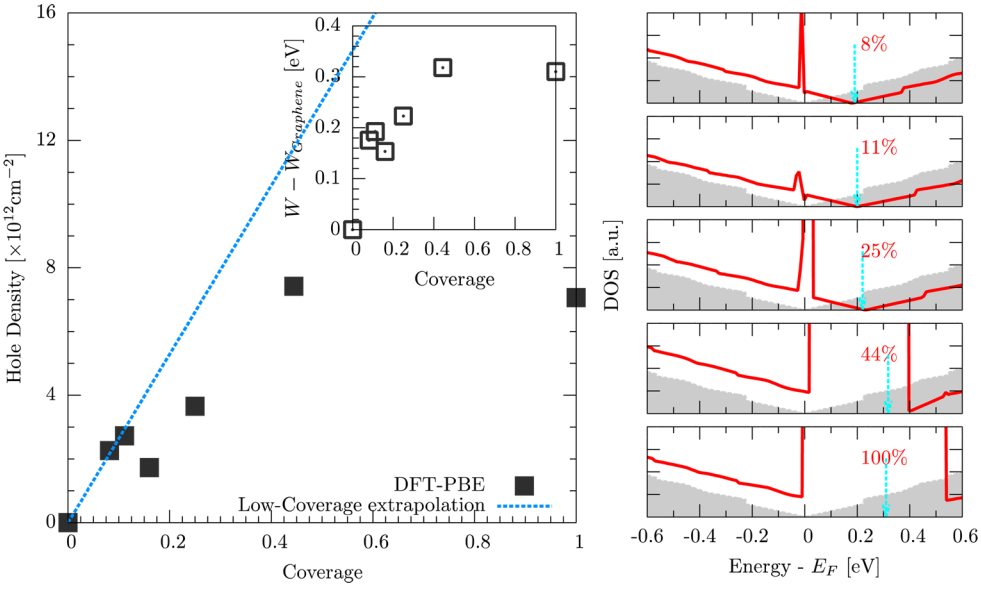

Figure 3. Computed hole densities and densities of states *versus* Br_2 coverage. (Left) The hole density is shown as a function of coverage for the b geometry (shown in ref 41), along with the linear extrapolation (blue dash) using the 8% coverage density. (Inset) Corresponding work functions on the graphene-terminated surface. (Right) Densities of states (red lines) for coverages varying from 8% to 100%. The density of states of the bare graphene is indicated in gray, for comparison. The energies of the Dirac point as determined from the work function shift on the graphene-terminated face are indicated in cyan.

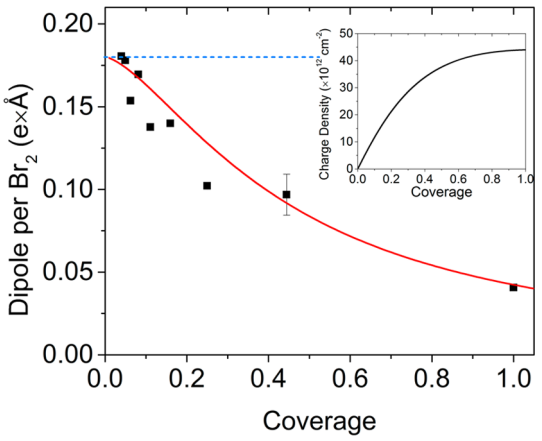

Figure 4. Calculated Dipole between graphene and Br_2 *versus* Br_2 coverage. The black squares denote dipoles from DFT calculation averaged over all 5 possible in-plane geometries, with the corresponding error bars estimated as the standard deviation of 5 geometries. The red line represents the fitting of the electrostatic model eq 1 to the calculated dipole, yielding an isolated dipole of 0.18 ± 0.01 e × Å and its polarizability of 35 ± 10 Å^3. The blue dash line shows a constant dipole if there is no interaction between neighboring dipoles. The inset graph shows the renormalized charge density *versus* Br_2 coverage. The curve was plotted from eq S5, using B = 1.8 determined from Figure S3 of the Supporting Information.

coverage. The densities of states plotted in Figure 3 show that the change in work function correlates with a shift of the Dirac point to positive energies, corresponding to a hole doping of the bare graphene. Moreover, they indicate that the Fermi energy of the system is pinned to the LUMO of Br_2. For coverages larger than 25% ($C_{32}Br_2$), we find that Br_2-Br_2 interactions lead to the formation of an energy band, with a bandwidth larger than 0.5 eV at 100%.

To understand the coverage dependence of the charge transfer, we show the computed areal dipole in Figure 4 as a function of coverage. In the far-field limit, the induced charge redistribution for each adsorbed Br_2 molecule can simply be modeled by a dipole p along the perpendicular direction. In the low-coverage limit, the interactions between neighboring dipoles are negligible, and the areal dipole increases linearly with coverage. As seen in Figure 4, for coverages larger than 6%, the independent-dipole model breaks down, and the Br_2-Br_2 interactions lead to an eventual decrease of the dipole at monolayer coverage. It is worth noticing that the breakdown of the independent dipole model appears at much lower coverages than the bandwidth associated with overlap of the Br_2 wave functions (negligible below 25%). Following Natan *et al.*,[30] we find that the deviation from the independent-dipole model is well reproduced by considering a polarizable dipole model, in which the dipole reads

$$p = \frac{p_0}{1 + \alpha k\theta^{3/2}/(2a)^3} \quad (1)$$

Here the dipole p_0 in the low coverage limit is depolarized by the mean-field through the term α (the dipole polarizability). k is a geometrical constant determined by the packing of Br_2 molecules (k = 11.034 in our study). a is the graphene unit cell length (2.46 Å). A best fit of this formula to the theoretical DFT dipoles in Figure 4 yields a polarizability of 35 ± 10 Å^3. The model of Natan *et al.*[30] should break down for high coverages[31] where interactions involving higher moments of the electronic density become important. Nevertheless, we find in practice that the deviation from the self-consistent result at 100% coverage to be less than 5%. Moreover, we find that the polarizable-dipole model leads to the correct functional form for the hole density: as seen in Supporting Information, we find a linear relationship between the charge density and areal dipole in the DFT calculations, with a parameter fit corresponding to a dipole length of 3.0 Å (80% of the calculated Br_2-graphene equilibrium distance, 3.77 Å).

It is worth noticing that the hole density extracted from DFT-PBE at full coverage (7.1×10^{12} cm^{-2}) significantly underestimates the experimental value (4.4×10^{13} cm^{-2}). This difference is not affected by the inclusion of the supporting h-BN layers in the modeling of the system. We attribute this behavior to the use of the geometries of reference[29] calculated with the vdW-DF functional which tends to overestimate the binding distances while leading to correct binding energies (as consequence of excessively repulsive exchange interactions[32−34]). We have verified (see Supporting Information, Figure S4) that decreasing the Br_2-graphene distance by 1.0 Å leads to enhanced charge transfer by more than 100%. Nevertheless, since the dependence of the charge transfer on Br_2 coverage results from long-range electrostatic interactions, we do not expect that any of these two issues would affect the functional form derived from DFT-PBE.

We did a renormalization to rescale the maximum charge density, retaining the large variation with coverage, shown in Figure 4. The coverage-dependence of charge density in Figure 4 converts Figure 2 to the absorption isotherm (coverage θ *versus* pressure P) shown in Figure 5. At full coverage, the rescaled charge density corresponds to a Fermi level 0.77 eV below the Dirac point.

To understand this adsorption isotherm, we first compare with the ideal Langmuir model, $\theta = KP/(1 + KP)$, which neglects interaction between adsorbed species. K is the equilibrium constant of the dynamic surface adsorption. While the general shape is correct, there is deviation in both high and low pressure regions. This deviation has its origin (at least in part) in the strong lateral interaction shown in the DFT calculation. The Fowler−Guggenheim (FG) isotherm, $KP = \theta/(1 - \theta)\exp(zw\theta/kT)$, assumes that randomly distributed adsorbate molecules interact with energy w if they are nearest

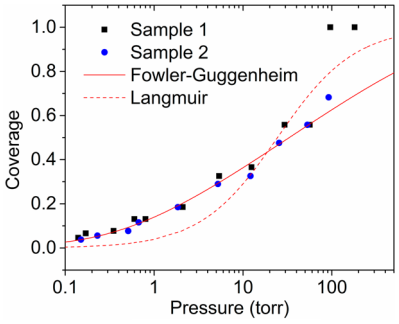

Figure 5. Br_2 adsorption isotherm on h-BN supported single-layer graphene. The red solid and dash lines delineate the fits using Fowler–Guggenheim and Langmuir adsorption models, respectively. These two adsorption models are discussed in the text.

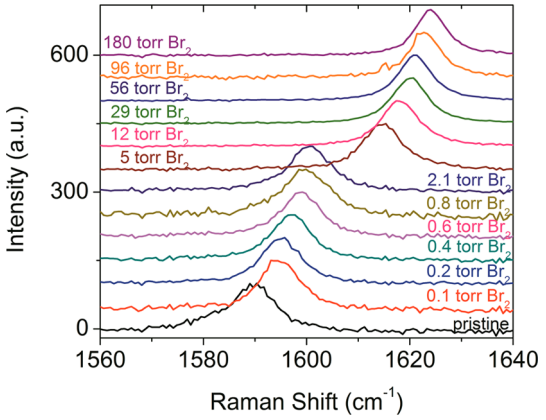

Figure 6. Raman spectra of SiO_2 supported single-layer graphene exposed to Br_2 at various pressures. The exposure started from the lowest pressure and gradually increased.

neighbors.[35] Here, z is the number of nearest-neighbor molecules (taken as 6 for Br_2 on graphene), a positive (or negative) w indicates repulsive (or attractive) interaction, k is the Boltzmann constant, and T is the surface temperature during the adsorption. Fitting this isotherm to our data gives a better agreement for equilibrium constant K 0.31 $\pm$ 0.03 $Torr^{-1}$ and lateral repulsive interaction w 20 $\pm$ 2 meV.

We can roughly estimate the binding energy E_b of Br_2 to graphene from the equilibrium constant K. While a precise determination of E_b requires a temperature-dependent study of K, an estimation of E_b is possible in the low pressure limit when coverage is equal to pressure multiplied by the equilibrium constant K.[36] Coverage can also be expressed as a product of gas flux rate and the lifetime of adsorbed molecules, which in turn can be related to the binding energy E_b.[36] By assuming the attempt frequency on the order of 10^{-12} s^{-1} and the adsorption site density to be the same as the intercalated planar Br_2 density of the stage-2 graphite intercalation compound studied by Dresselhaus,[14] E_b is estimated as ~350 meV for Br_2 on h-BN supported graphene. The value agrees well with DFT calculation of E_b (285 – 296 meV).[29] With these assumptions, each Br_2 molecule is estimated to accept 0.09 e^- from graphene at full coverage, which agrees reasonably well with the DFT result (0.045 e^-).[29]

Thus, for the case of flat graphene supported on h-BN, we have a partial understanding of gaseous Br_2 surface adsorption and charge transfer. The Br_2 binding energy is 350 meV, an order of magnitude higher than thermal energy at room temperature. The net binding between graphene and a Br_2 monolayer of 1.7 eV/nm^2 is similar to the 2.0 $\pm$ 0.2 eV/nm^2 (or 52 $\pm$ 5 meV per C atom)[37] van der Waals binding between two graphene layers. A Langmuir adsorption isotherm is not observed mainly because of strong lateral interaction (depolarization) between adsorbed molecules. The charge transfer per adsorbed Br_2 decreases by about at factor of 2 as adsorption proceeds toward a full monolayer. The net charge transfer for a Br_2 monolayer is still relatively high -4.4×10^{13} holes/cm^2, corresponding to 0.09 e^- per adsorbed molecule. Curiously, this value for an adsorbed monolayer is larger than the range of values reported for intercalated layers: 0.019 $\pm$ 0.003 by the Dresselhaus group,[38] and 0.023 by the Hebard group.[16] In our previous report,[13] 2L and 4L graphenes show the same G peak position after exposure to high pressure Br_2 (forming stage-2 compound), indicating that net charge transfer from one intercalant Br_2 layer is similar to two adsorbed layers. Thus, intercalated Br_2 is expected to accept twice as much charge as the adsorbed one. The significance of these observations is not clear.

Graphene supported on SiO_2 shows significantly different behavior. In Figure 6, graphene is initially hole-doped on SiO_2 compared to that on h-BN. Such initial doping comes from the charge impurities in SiO_2 and is consistent with previous reports.[24,26,39] We treat the initial doping as residue doping and remove it from the doping after Br_2 exposure. Furthermore, the plot of G peak position *versus* Br_2 pressure shows a significant jump between 2 and 5 Torr. This break, not seen on h-BN substrate, varies somewhat from sample to sample. We assign this discontinuity to the existence of a threshold pressure for Br_2 vapor diffusion into the sample-dependent interface between graphene and SiO_2. The graphene-SiO_2 contact is point-like and loose, since untreated mechanically exfoliated graphene is thought to sit just on the high points of the somewhat rough SiO_2 surface.[40] At high pressure *ca.* 100 Torr, the limiting charge density n_{max} is about 7.1×10^{13} cm^{-2}, larger than h-BN supported value by ~60%. The increase comes from the contribution of Br_2 molecules trapped at the graphene-SiO_2 interface. The binding of Br_2 at the oxide/graphene interface may be stabilized by the charge impurities presented in SiO_2.

In a heuristic treatment, to separate contributions from the top-side adsorption and interfacial adsorption, we assume that the doping from top Br_2 layer on SiO_2 supported graphene is close to that of h-BN

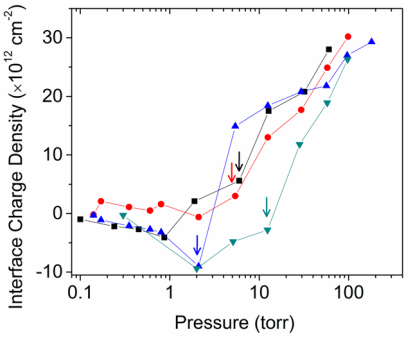

Figure 7. Interface charge density introduced by Br_2 trapped between graphene and SiO_2 as a function of Br_2 pressure. The total charge density was calculated from the G peak position in Figure 6. The exposed side is approximated as the same of graphene on h-BN. The difference yields the interface charge density. Four samples were measured independently with threshold pressure indicated by the arrows indicate.

supported graphene as shown in Figure 2. Specifically, to estimate the top-side contribution, we extract the coverage from the Fowler–Guggenheim absorption isotherm in Figure 5 and calculate the charge density using eq S5 in Supporting Information. After calculating the total charge density from G peak position and subtracting the contribution from the top layer, we estimated the amount of interfacial Br_2 molecules. We neglect repulsion between top and interfacial Br_2 layers. This treatment might provide some insight into the diffusion of Br_2 into the interface at low coverage where repulsion does not play a significant role. As shown in Figure 7, arrows indicate individual threshold pressure for four samples below which the interfacial amount of Br_2 is negligible and Br_2 is only adsorbed on the top (or unsupported) side of graphene. The threshold pressure varies with sample in the range of 2–12 Torr. As discussed previously, such variation is also an indicator of ill-defined interface between graphene and rough amorphous SiO_2 surface, compared to graphene on h-BN.

In summary, bromine adsorption behavior on graphene depends strongly on the underlying substrate. Previously, the diffusion and nucleation behavior of adsorbed Au atoms was also seen to be strongly dependent on the underlying substrate.[41] 2D graphene is sensitive to the local environment, showing essentially molecular behavior in this regard, as every atom is on the surface.

CONCLUSIONS

By monitoring the charge transfer from graphene to adsorbed Br_2 molecules using Raman spectroscopy, we observed different adsorption behaviors on graphene. Br_2 is only adsorbed on the unsupported side of graphene on h-BN, while both sides of graphene are covered with Br_2 when placed on SiO_2 at high pressure. Even though graphene forms only loose contact with SiO_2, a threshold pressure is still required for Br_2 molecules to diffuse into the interface. Combining Raman spectroscopy and DFT calculation, we present the adsorption isotherm of Br_2 on h-BN supported graphene. From the isotherm, we estimated the binding energy (~0.35 eV) of adsorbed Br_2 to graphene and the lateral repulsion energy (~20 meV) between Br_2 molecules.

METHODS

For SiO_2 supported graphene, graphene was mechanically exfoliated[42] onto Si/SiO_2 substrates. A transfer technique was employed to fabricate graphene on h-BN and h-BN/graphene/h-BN sandwich structure.[24,43] The procedure of Br_2 exposure can be found in a previous report.[13] The graphene sample was kept inside a sealed quartz cuvette. The Br_2 pressure in the cuvette was varied by changing the temperature of a liquid Br_2 reservoir. We used UV–vis spectroscopy to determine the pressure of Br_2 in the cuvette.[44] The Raman spectra were collected in the backscattering geometry with a 40× objective through the cuvette wall. The samples were illuminated using a 632.8 nm laser with power less than 1 mW at the sample plane. The spectral resolution was ~2 cm^{-1}.

All DFT calculations[45,46] were performed using the Vienna *ab initio* simulation package (VASP).[47–50] We used the generalized gradient approximation of Perdew, Burke, and Ernzerhof in its nonspin-polarized formulation.[51] The Kohn–Sham equations are solved using a plane-wave basis set with a kinetic energy cutoff of 500 eV using the projector augmented wave method.[52,53] Out-of-plane lattice vector length is chosen to be 40 Å and a dipole correction is applied in order to cancel out the long-range interactions along this axis. For all coverage, the Brillouin zone is mapped with in-plane k-point densities corresponding to a 72 × 72 mesh in the primitive cell. Coverage effects are modeled by using a range of supercells going from a 3 × 3 × 1 to a 10 × 10 × 1 using the geometries (a)–(e) of ref 41 for which Br_2 lies flat at distances of 3.74–3.77 Å above the plane of graphene (modeled at its experimental lattice parameter). The "full coverage" limit is taken from ref 14 and corresponds to a Br_2 molecule for 8 carbon atoms. For graphene supported by h-BN, the graphene layer is fixed at 3.35 Å above 6 layers of h-BN (interlayer separation 3.34 Å) with an in-plane lattice vector stretched to the graphene value.

Conflict of Interest: The authors declare no competing financial interest.

Acknowledgment. We would like to thank fruitful discussions with Y. Guo, E. S. Thrall, F. Varchon, M. Kotiuga, J. B. Neaton, L.Venkataraman, and H. Wang, and experimental assistant from S. Jockusch and S. Berciaud. Theoretical work by P.D. and C.A.M. was supported by the MIRT grant NSF DMR-1122594. This research utilized resources at the New York Center for Computational Sciences at Stony Brook University/Brookhaven National Laboratory which is supported by the U.S. Department of Energy under Contract No. DE-AC02-98CH10886 and by the State of New York. Experimental work was supported by National Science Foundation through the MIRT program (Grant No. DMR-1122594).

Supporting Information Available: Additional Raman spectra, plots of charge density *versus* Br_2 pressure, and the correlation between graphene charge density and Br_2 coverage on graphene. This material is available free of charge *via* the Internet at http://pubs.acs.org.

REFERENCES AND NOTES

1. Novoselov, K. S.; Geim, A. K.; Morozov, S. V.; Jiang, D.; Zhang, Y.; Dubonos, S. V.; Grigorieva, I. V.; Firsov, A. A. Electric Field Effect in Atomically Thin Carbon Films. *Science* **2004**, *306*, 666–669.
2. Zhang, Y. B.; Tan, Y. W.; Stormer, H. L.; Kim, P. Experimental Observation of the Quantum Hall Effect and Berry's Phase in Graphene. *Nature* **2005**, *438*, 201–204.
3. Geim, A. K.; Novoselov, K. S. The Rise of Graphene. *Nat. Mater.* **2007**, *6*, 183–191.
4. Bolotin, K. I.; Sikes, K. J.; Jiang, Z.; Klima, M.; Fudenberg, G.; Hone, J.; Kim, P.; Stormer, H. L. Ultrahigh Electron Mobility in Suspended Graphene. *Solid State Commun.* **2008**, *146*, 351–355.
5. McCann, E. Asymmetry Gap in the Electronic Band Structure of Bilayer Graphene. *Phys Rev B* **2006**, *74*, 161403(R).
6. Castro, E. V.; Novoselov, K. S.; Morozov, S. V.; Peres, N. M. R.; Dos Santos, J. M. B. L.; Nilsson, J.; Guinea, F.; Geim, A. K.; Neto, A. H. C. Biased Bilayer Graphene: Semiconductor with a Gap Tunable by the Electric Field Effect. *Phys. Rev. Lett.* **2007**, *99*, 216802.
7. Zhang, Y. B.; Tang, T. T.; Girit, C.; Hao, Z.; Martin, M. C.; Zettl, A.; Crommie, M. F.; Shen, Y. R.; Wang, F. Direct Observation of a Widely Tunable Bandgap in Bilayer Graphene. *Nature* **2009**, *459*, 820–823.
8. Yan, J.; Fuhrer, M. S. Charge Transport in Dual Gated Bilayer Graphene with Corbino Geometry. *Nano Lett.* **2010**, *10*, 4521–4525.
9. Yu, W. J.; Liao, L.; Chae, S. H.; Lee, Y. H.; Duan, X. F. Toward Tunable Band Gap and Tunable Dirac Point in Bilayer Graphene with Molecular Doping. *Nano Lett.* **2011**, *11*, 4759–4763.
10. Zhang, W. J.; Lin, C. T.; Liu, K. K.; Tite, T.; Su, C. Y.; Chang, C. H.; Lee, Y. H.; Chu, C. W.; Wei, K. H.; Kuo, J. L.; *et al.* Opening an Electrical Band Gap of Bilayer Graphene with Molecular Doping. *ACS Nano* **2011**, *5*, 7517–7524.
11. Park, J.; Jo, S. B.; Yu, Y. J.; Kim, Y.; Yang, W.; Lee, W. H.; Kim, H. H.; Hong, B. H.; Kim, P.; Cho, K.; *et al.* Single-Gate Bandgap Opening of Bilayer Graphene by Dual Molecular Doping. *Adv. Mater. (Weinheim, Ger.)* **2012**, *24*, 407–411.
12. Jung, N.; Kim, B.; Crowther, A. C.; Kim, N.; Nuckolls, C.; Brus, L. Optical Reflectivity and Raman Scattering in Few-Layer-Thick Graphene Highly Doped by K and Rb. *ACS Nano* **2011**, *5*, 5708–5716.
13. Jung, N.; Kim, N.; Jockusch, S.; Turro, N. J.; Kim, P.; Brus, L. Charge Transfer Chemical Doping of Few Layer Graphenes: Charge Distribution and Band Gap Formation. *Nano Lett.* **2009**, *9*, 4133–4137.
14. Dresselhaus, M. S.; Dresselhaus, G. Intercalation Compounds of Graphite. *Adv. Phys.* **2002**, *51*, 1–186.
15. Tongay, S.; Hwang, J.; Tanner, D. B.; Pal, H. K.; Maslov, D.; Hebard, A. F. Supermetallic Conductivity in Bromine-Intercalated Graphite. *Phys. Rev. B* **2010**, *81*, 115428.
16. Hwang, J.; Carbotte, J. P.; Tongay, S.; Hebard, A. F.; Tanner, D. B. Ultrapure Multilayer Graphene in Bromine-Intercalated Graphite. *Phys. Rev. B* **2011**, *84*, 041410(R).
17. Crowther, A. C.; Ghassaei, A.; Jung, N.; Brus, L. E. Strong Charge-Transfer Doping of 1 to 10 Layer Graphene by No2. *ACS Nano* **2012**, *6*, 1865–1875.
18. Ando, T.; Koshino, M. Field Effects on Optical Phonons in Bilayer Graphene. *J. Phys. Soc. Jpn.* **2009**, *78*, 034709.
19. Yan, J.; Villarson, T.; Henriksen, E. A.; Kim, P.; Pinczuk, A. Optical Phonon Mixing in Bilayer Graphene with a Broken Inversion Symmetry. *Phys. Rev. B* **2009**, *80*, 241417(R).
20. Yan, J.; Zhang, Y. B.; Kim, P.; Pinczuk, A. Electric Field Effect Tuning of Electron-Phonon Coupling in Graphene. *Phys. Rev. Lett.* **2007**, *98*, 166802.
21. Das, A.; Pisana, S.; Chakraborty, B.; Piscanec, S.; Saha, S. K.; Waghmare, U. V.; Novoselov, K. S.; Krishnamurthy, H. R.; Geim, A. K.; Ferrari, A. C.; *et al.* Monitoring Dopants by Raman Scattering in an Electrochemically Top-Gated Graphene Transistor. *Nat. Nanotechnol.* **2008**, *3*, 210–215.
22. Das, A.; Chakraborty, B.; Piscanec, S.; Pisana, S.; Sood, A. K.; Ferrari, A. C. Phonon Renormalization in Doped Bilayer Graphene. *Phys. Rev. B* **2009**, *79*, 155417.
23. Chen, C. F.; Park, C. H.; Boudouris, B. W.; Horng, J.; Geng, B. S.; Girit, C.; Zettl, A.; Crommie, M. F.; Segalman, R. A.; Louie, S. G.; *et al.* Controlling Inelastic Light Scattering Quantum Pathways in Graphene. *Nature* **2011**, *471*, 617–620.
24. Wang, L.; Chen, Z.; Dean, C. R.; Taniguchi, T.; Watanabe, K.; Brus, L. E.; Hone, J. Negligible Environmental Sensitivity of Graphene in a Hexagonal Boron Nitride/Graphene/H-Bn Sandwich Structure. *ACS Nano* **2012**, *6*, 9314–9319.
25. Watanabe, K.; Taniguchi, T.; Kanda, H. Direct-Bandgap Properties and Evidence for Ultraviolet Lasing of Hexagonal Boron Nitride Single Crystal. *Nat. Mater.* **2004**, *3*, 404–409.
26. Dean, C. R.; Young, A. F.; Meric, I.; Lee, C.; Wang, L.; Sorgenfrei, S.; Watanabe, K.; Taniguchi, T.; Kim, P.; Shepard, K. L.; *et al.* Boron Nitride Substrates for High-Quality Graphene Electronics. *Nat. Nanotechnol.* **2010**, *5*, 722–726.
27. Xue, J. M.; Sanchez-Yamagishi, J.; Bulmash, D.; Jacquod, P.; Deshpande, A.; Watanabe, K.; Taniguchi, T.; Jarillo-Herrero, P.; Leroy, B. J. Scanning Tunnelling Microscopy and Spectroscopy of Ultra-Flat Graphene on Hexagonal Boron Nitride. *Nat. Mater.* **2011**, *10*, 282–285.
28. Decker, R.; Wang, Y.; Brar, V. W.; Regan, W.; Tsai, H. Z.; Wu, Q.; Gannett, W.; Zettl, A.; Crommie, M. F. Local Electronic Properties of Graphene on a Bn Substrate *via* Scanning Tunneling Microscopy. *Nano Lett.* **2011**, *11*, 2291–2295.
29. Rudenko, A. N.; Keil, F. J.; Katsnelson, M. I.; Lichtenstein, A. I. Adsorption of Diatomic Halogen Molecules on Graphene: A van der Waals Density Functional Study. *Phys. Rev. B* **2010**, *82*, 035427.
30. Natan, A.; Kronik, L.; Haick, H.; Tung, R. T. Electrostatic Properties of Ideal and Non-Ideal Polar Organic Monolayers: Implications for Electronic Devices. *Adv. Mater. (Weinheim, Ger.)* **2007**, *19*, 4103–4117.
31. Kotiuga, M.; Darancet, P.; Arroyo, C.; Venkataraman, L.; Neaton, J. B. Quantitative Impact of Solvent on Charge Transport in Molecular Junctions. Unpublished.
32. Klimes, J.; Bowler, D. R.; Michaelides, A. Chemical Accuracy for the van der Waals Density Functional. *J. Phys.: Condens. Matter* **2010**, *22*, 022201.
33. Cooper, V. R. van der Waals Density Functional: An Appropriate Exchange Functional. *Phys. Rev. B* **2010**, *81*, 161104.
34. Lee, K.; Murray, É. D.; Kong, L.; Lundqvist, B. I.; Langreth, D. C. Higher-Accuracy van der Waals Density Functional. *Phys. Rev. B* **2010**, *82*, 081101.
35. Fowler, R. H.; Guggenheim, E. A. *Statistical Thermodynamics*; Cambridge University Press: London, 1939; p 429−433.
36. Somorjai, G. A.; Li, Y., *Introduction to Surface Chemistry and Catalysis*, 2nd ed.; John Wiley & Sons, Inc.: Hoboken, NJ, 2010; p 314−315.
37. Zacharia, R.; Ulbricht, H.; Hertel, T. Interlayer Cohesive Energy of Graphite from Thermal Desorption of Polyaromatic Hydrocarbons. *Phys. Rev. B* **2004**, *69*, 155406.
38. Platts, D. A.; Chung, D. D. L.; Dresselhaus, M. S. Far-Infrared Magnetoreflection Studies of Graphite Intercalated with Bromine. *Phys. Rev. B* **1977**, *15*, 1087–1092.
39. Casiraghi, C.; Pisana, S.; Novoselov, K. S.; Geim, A. K.; Ferrari, A. C. Raman Fingerprint of Charged Impurities in Graphene. *Appl. Phys. Lett.* **2007**, *91*, 233108.
40. Ryu, S.; Liu, L.; Berciaud, S.; Yu, Y. J.; Liu, H. T.; Kim, P.; Flynn, G. W.; Brus, L. E. Atmospheric Oxygen Binding and Hole Doping in Deformed Graphene on a Sio_2 Substrate. *Nano Lett.* **2010**, *10*, 4944–4951.
41. Liu, L.; Chen, Z. Y.; Wang, L.; Polyakova, E.; Taniguchi, T.; Watanabe, K.; Hone, J.; Flynn, G. W.; Brus, L. E. Slow Gold Adatom Diffusion on Graphene: Effect of Silicon Dioxide and Hexagonal Boron Nitride Substrates. *J. Phys. Chem. B* **2013**, *117*, 4305–4312.
42. Novoselov, K. S.; Jiang, D.; Schedin, F.; Booth, T. J.; Khotkevich, V. V.; Morozov, S. V.; Geim, A. K. Two-Dimensional Atomic Crystals. *Proc. Natl. Acad. Sci. U. S. A.* **2005**, *102*, 10451–10453.
43. Wang, L.; Meric, I.; Huang, P. Y.; Gao, Q.; Gao, Y.; Tran, H.; Taniguchi, T.; Watanabe, K.; Campos, L. M.; Muller, D. A.; *et al.*

One-Dimensional Electrical Contact to a Two-Dimensional Material. *Science* **2013**, *342*, 614–617.
44. Maric, D.; Burrows, J. P.; Moortgat, G. K. A Study of the Uv-Visible Absorption-Spectra of Br-2 and Brcl. *J. Photochem Photobiol., A* **1994**, *83*, 179–192.
45. Hohenberg, P.; Kohn, W. Inhomogeneous Electron Gas. *Phys. Rev.* **1964**, *136*, B864–B871.
46. Kohn, W.; Sham, L. J. Self-Consistent Equations Including Exchange and Correlation Effects. *Phys. Rev.* **1965**, *140*, A1133–A1138.
47. Kresse, G.; Hafner, J. *Ab Initio* Molecular Dynamics for Liquid Metals. *Phys. Rev. B* **1993**, *47*, 558–561.
48. Kresse, G.; Hafner, J. *Ab Initio* Molecular-Dynamics Simulation of the Liquid-Metal Amorphous-Semiconductor Transition in Germanium. *Phys. Rev. B* **1994**, *49*, 14251–14269.
49. Kresse, G.; Furthmuller, J. Efficiency of *ab Initio* Total Energy Calculations for Metals and Semiconductors Using a Plane-Wave Basis Set. *Comput. Mater. Sci.* **1996**, *6*, 15–50.
50. Kresse, G.; Furthmuller, J. Efficient Iterative Schemes for *Ab Initio* Total-Energy Calculations Using a Plane-Wave Basis Set. *Phys. Rev. B* **1996**, *54*, 11169–11186.
51. Perdew, J. P.; Burke, K.; Ernzerhof, M. Generalized Gradient Approximation Made Simple. *Phys. Rev. Lett.* **1996**, *77*, 3865–3868.
52. Blochl, P. E. Projector Augmented-Wave Method. *Phys. Rev. B* **1994**, *50*, 17953–17979.
53. Kresse, G.; Joubert, D. From Ultrasoft Pseudopotentials to the Projector Augmented-Wave Method. *Phys. Rev. B* **1999**, *59*, 1758–1775.